



## LJMU Research Online

Duffy, SJ, Benbakhti, B, Kalna, K, Boucherta, M, Zhang, WD, Bourzgui, N and Soltani, A

**Strain-Reduction Induced Rise in Channel Temperature at Ohmic Contacts of GaN HEMTs**

<http://researchonline.ljmu.ac.uk/id/eprint/9079/>

### Article

**Citation** (please note it is advisable to refer to the publisher's version if you intend to cite from this work)

**Duffy, SJ, Benbakhti, B, Kalna, K, Boucherta, M, Zhang, WD, Bourzgui, N and Soltani, A (2018) Strain-Reduction Induced Rise in Channel Temperature at Ohmic Contacts of GaN HEMTs. IEEE Access. ISSN 2169-3536**

LJMU has developed [LJMU Research Online](#) for users to access the research output of the University more effectively. Copyright © and Moral Rights for the papers on this site are retained by the individual authors and/or other copyright owners. Users may download and/or print one copy of any article(s) in LJMU Research Online to facilitate their private study or for non-commercial research. You may not engage in further distribution of the material or use it for any profit-making activities or any commercial gain.

The version presented here may differ from the published version or from the version of the record. Please see the repository URL above for details on accessing the published version and note that access may require a subscription.

For more information please contact [researchonline@ljmu.ac.uk](mailto:researchonline@ljmu.ac.uk)

<http://researchonline.ljmu.ac.uk/>

Received May 31, 2018, accepted July 6, 2018. Date of publication xxxx 00, 0000, date of current version xxxx 00, 0000.

Digital Object Identifier 10.1109/ACCESS.2018.2861323

# Strain-Reduction Induced Rise in Channel Temperature at Ohmic Contacts of GaN HEMTs

STEVEN J. DUFFY<sup>1</sup>, BRAHIM BENBAKHTI<sup>1</sup>, (Member, IEEE),  
KAROL KALNA<sup>2</sup>, (Fellow, IEEE), MOHAMMED BOUCHERTA<sup>3</sup>,  
WEI D. ZHANG<sup>1</sup>, NOUR E. BOURZGUI<sup>3</sup>, AND ALI SOLTANI<sup>3,4</sup>

<sup>1</sup>Department of Electronics and Electrical Engineering, Liverpool John Moores University, Liverpool L3 3AF, U.K.

<sup>2</sup>Nanoelectronic Devices Computational Group, College of Engineering, Swansea University, Swansea SA1 8EN, U.K.

<sup>3</sup>Institute of Electronics, Microelectronics and Nanotechnology, Université de Lille 1, 59650 Villeneuve-d'Ascq, France

<sup>4</sup>Laboratoire Nanotechnologies Nanosystèmes, Université de Sherbrooke, Sherbrooke, QC J1K 0A5, Canada

Corresponding author: Brahim Benbakhti (b.benbakhti@ljamu.ac.uk)

This work was supported by the Department of Electronics and Electrical Engineering, Liverpool John Moores University, Liverpool L3 3AF, U.K.

**ABSTRACT** Operating temperature distributions in AlGaIn/GaN gateless and gated devices are characterized and analyzed using the InfraScope temperature mapping system. For the first time, a substantial rise of channel temperature at the inner ends of ohmic contacts has been observed. Synchrotron radiation-based high-resolution X-ray diffraction technique combined with drift-diffusion simulations show that strain reduction at the vicinity of ohmic contacts increases electric field at these locations, resulting in the rise of lattice temperature. The thermal coupling of a high conductive tensile region at the contacts to a low conductive channel region is an origin of the temperature rise observed in both short- and long-channel gateless devices.

**INDEX TERMS** AlGaIn/GaN based devices, ohmic contact, self-heating, infrared camera, high-resolution X-ray diffraction.

## I. INTRODUCTION

AlGaIn/GaN based devices are promising candidates for high-power and high-frequency applications [1]–[3]. These devices can be manufactured onto the existing Silicon substrates, allowing co-integration with conventional Silicon technology. The wide bandgap, high electron velocity saturation, and good thermal conductivity of III-Nitrides (III-N) provide distinctive advantages over the conventionally used Silicon, leading to superior high-power and high-frequency device performance [1], [2]. However, the superior performance of AlGaIn/GaN High Electron Mobility Transistors (HEMTs) is hampered by serious reliability issues, which are holding back their widespread commercial and industrial development. Deleterious phenomena such as: (i) self-heating effects, that significantly impact the transport properties in the semiconductor, (ii) charge trapping effects, that are responsible for reducing device lifetime and reliability, and (iii) source/drain Ohmic contact (S/D) resistances increase during device operation, are controversial with unclear physics [4]–[6]. These accelerating factors are behind device performance degradation and persist to be limiting reliability factors [4]–[6]. Maintaining high performance and reliability of the S/D Ohmic contacts in AlGaIn/GaN HEMTs is a significant challenge, particularly

at high operating voltage, which hinders progress in a large-scale deployment of the technology in applications [4]–[6].

In this work, we investigate the channel temperature distribution in AlGaIn/GaN based devices using Infrascopes temperature mapping system (IR) accompanied by synchrotron radiation-based High-Resolution X-RAY Diffraction (HRXRD) measurements and physically based TCAD simulations, for the first time. This unique approach demonstrates that compressive and tensile strain around S/D contacts affects temperature distribution during device operation and limiting its performance. Section II overviews devices under investigation and experimental procedure. Section III presents channel temperature profiles in the devices under different configurations and examines physics behind temperature rise at the S/D contacts of gateless devices. Conclusions are drawn in Section IV.

## II. DEVICES AND EXPERIMENTAL PROCEDURE

The investigated epi-structure has been grown by molecular beam epitaxy on High-Purity HP-Si(111) substrate (Fig. 1). It consists, from the substrate to the top surface, of low-temperature AlN(40 nm)/GaN(250 nm)/AlN(250 nm) nucleation layers, a 1.7  $\mu\text{m}$  Al<sub>0.10</sub>Ga<sub>0.90</sub>N back-barrier to reduce leakage current in the buffer and to improve

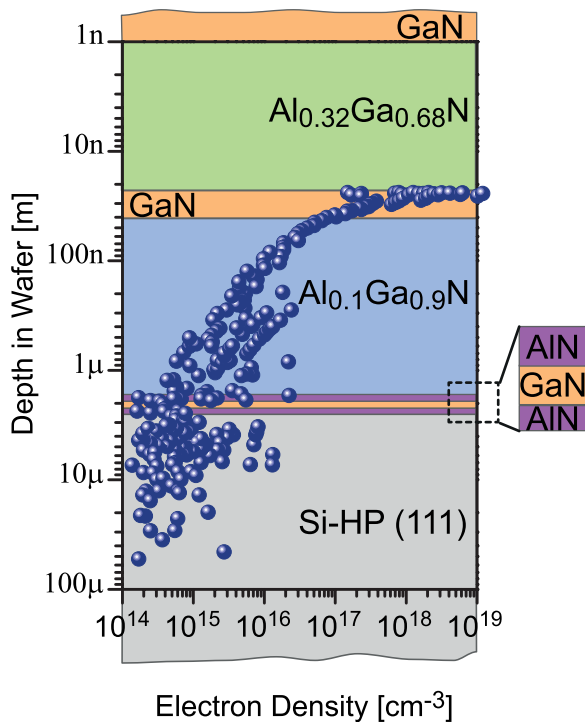


**FIGURE 1.** Epi-structure and measured electron density profile of the investigated wafer, GaN(1nm)/Al<sub>0.32</sub>Ga<sub>0.68</sub>N(25nm)/GaN(15nm)/Al<sub>0.10</sub>Ga<sub>0.90</sub>N(1.7μm)/NL/HP-Si(111), where NL are nucleation layers that consist of AlN(40nm)/GaN(250nm)/AlN(250nm).

the carrier confinement of the 2-dimensional electron gas (2DEG). A channel is made of a 15 nm thick unintentionally doped GaN buffer followed by a 25 nm undoped Al<sub>0.32</sub>Ga<sub>0.68</sub>N barrier and, finally, a 1 nm GaN cap layer. Room temperature Hall measurements yield a 2DEG electron mobility of 1750 cm<sup>2</sup> V<sup>-1</sup>s<sup>-1</sup> and  $R_{\square} = 310 \Omega/\square$ . The CV-technique revealed an electron sheet density of  $1.18 \times 10^{13} \text{ cm}^{-2}$  in the buffer. The fabrication process flow is similar to that in [7]. To reduce the contact resistance, the S/D terminals are formed by rapid thermal annealing of an evaporated Ti(10nm)/Al(200nm)/Ni(40nm)/Au(100nm) multilayers metallization scheme at 870°C for 30 s under nitrogen atmosphere. The S/D contacts resistance and specific resistivity are 0.39  $\Omega\cdot\text{mm}$  and  $3.8 \times 10^{-6} \Omega\cdot\text{cm}^2$ , respectively. The devices are electrically isolated by He<sup>+</sup> ion multiple implantations. To reduce trapping effects and dispersion, the surface of the devices are N<sub>2</sub>O pre-treated for 2 min followed by SiO<sub>2</sub>(100nm)/Si<sub>3</sub>N<sub>4</sub>(50nm) bi-layer passivation, performed by plasma-enhanced chemical vapor deposition at 340°C. The SiO<sub>2</sub>(100nm)/Si<sub>3</sub>N<sub>4</sub>(50nm) bi-layer is opened by using a CHF<sub>3</sub>/CF<sub>4</sub> reactive ion etching plasma. The used gate metallization scheme is Ni(5nm)/Pt(25nm)/Ti(25nm)/Mo(30nm)/Au(250nm).

The electrical I-V characterizations are performed at DC and dark conditions using Agilent B1500A framework. Before taking any measurements,  $V_{DS} = 0 \text{ V}$  is applied for a period of time to fully recover the device from deleterious phenomena of charge trapping and self-heating that would

distort further measurements. The trace of drain current is reproducible showing that no permanent degradation of drain current occurs from the experiment, only recoverable degradation, i.e., charge trapping and self-heating.

To measure the temperature profile, our Infrascopes temperature mapping system, equipped with  $500 \times 500$  InSb detectors array, is first calibrated. A high emissivity layer is coated over the device and surface radiation of the unbiased AlGaIn/GaN device is measured, whilst increasing the temperature from 50°C to 200°C with a step of 15°C using a heated-stage to maintain constant uniform temperature [8], [9]. The surface temperature is then measured from the emissivity by comparing it with the instrument calibration curve (not shown). After the calibration step, each device is first placed on a constant temperature platform (40°C or 45°C) and biased at DC conditions using Agilent B1500A framework. Then, thermal imaging measurements are performed using the calibrated Infrascopes system. Pixel resolution of the obtained IR image is about 2.3  $\mu\text{m}$ , giving a total field of view of about 1 mm  $\times$  1 mm. This technique is based on measuring the IR radiations emitted at the top surface of the device that are proportional to the temperature.

The strain relaxation in the AlGaIn barrier layer of an unbiased device is measured using synchrotron radiation-based High-Resolution X-RAY Diffraction (HRXRD) [21]. This technique uses 10.4 keV energy at the 2-ID-D micro-diffraction beamline of the Advanced Photon Source (APS) at Argonne National Laboratory. The sample device is mounted on an XYZ stage with a 50 nm lateral resolution. The location of the beam spot was monitored by means of simultaneous measurement of Ga-K fluorescence intensities and the diffraction data were collected by a charge-coupled detector. The size of the quasi-circular beam spot is  $\approx 220 \text{ nm}$  with 180 arc sec divergence.

The electrostatic of the used devices has been investigated by Drift-Diffusion (DD) simulations. The details of the used device simulation technique can be found in [10] and [24]–[28]. In the past, this simulation technique has been successfully used to predict AlGaIn/GaN based device architectures grown on various substrates (i.e., Si, 4H-SiC, diamond, sapphire). The transport parameters such as electron drift velocity, energy relaxation time, and electron effective mass are obtained from Monte Carlo simulation runs at different lattice temperatures [28]. Both simulated I–V characteristics and calculated temperatures have been compared to experimental I–V characteristics and temperature measurements, demonstrating a good agreement [10], [24], [25], [27]. Moreover, this simulation technique has been adapted to deal with both gated and gateless AlGaIn/GaN devices.

### III. RESULTS AND DISCUSSION

#### A. AlGaIn/GaN GATELESS DEVICES

The  $I_D$ - $V_D$  characteristics of the used 100  $\mu\text{m}$  wide gateless AlGaIn/GaN Transmission Line Measurement structures (TLMs) with different source-to-drain distances,

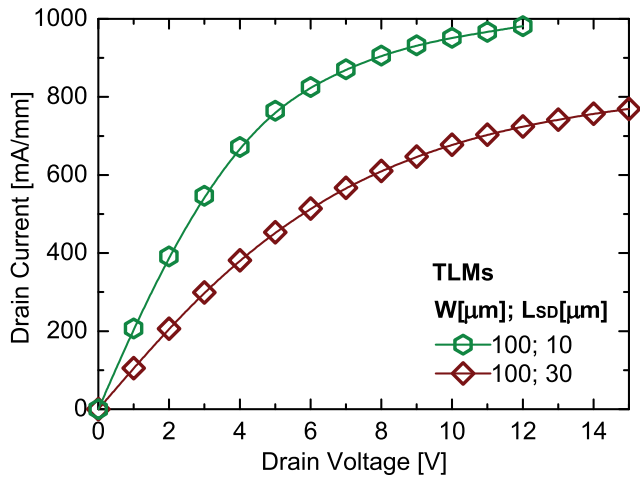


**FIGURE 2.** Measured  $I_D$ - $V_D$  characteristics of the gateless AlGaIn/GaN Transmission line measurement structures (TLMs). The source-to-drain distance of the used TLMs are  $L_{SD} = 10 \mu\text{m}$  (short TLM) and  $L_{SD} = 30 \mu\text{m}$  (long TLM).

$L_{SD} = 10 \mu\text{m}$  (short TLM) and  $L_{SD} = 30 \mu\text{m}$  (long TLM), are shown in Fig. 2. A lower current and a larger resistance are observed for the long TLM ( $L_{SD} = 30 \mu\text{m}$ ).

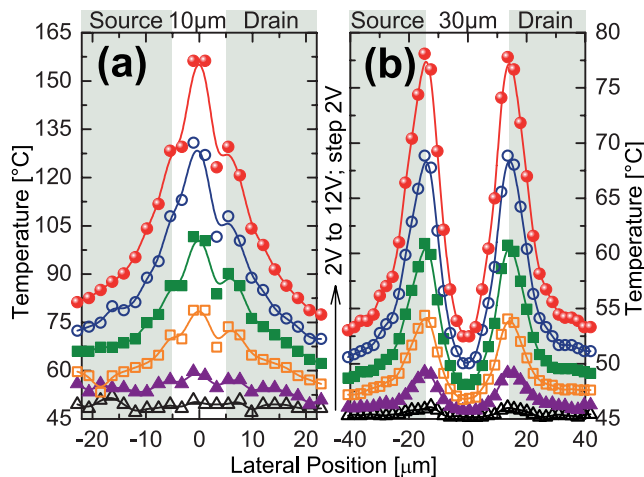


**FIGURE 3.** Measured temperature profiles along the top surface of the gateless AlGaIn/GaN structures at different drain voltages for (a) short TLM ( $L_{SD} = 10 \mu\text{m}$ ) and (b) long TLM ( $L_{SD} = 30 \mu\text{m}$ ).

Fig. 3 shows the temperature distributions along the surface of the short and long TLMs,  $L_{SD} = 10 \mu\text{m}$  and  $L_{SD} = 30 \mu\text{m}$ , at  $V_{DS} = 2 \text{ V}$  to  $12 \text{ V}$  by step of  $2 \text{ V}$ . For the long TLM, temperature peaks are observed at the inner ends of the S/D contacts, for all applied biases (Fig. 3b). These temperature peaks merge when  $L_{SD}$  decreases as a result of temperature coupling (Fig. 3a). For  $L_{SD} \leq 10 \mu\text{m}$ , the amount of thermal coupling between the source and the drain sides is even larger making it difficult to observe the temperature peaks at the inner end of the Ohmic contacts (not shown). Note that this thermal coupling induced temperature rise can significantly impact the device performance through

increase in the contact access resistance and electron mobility degradation, particularly for small devices, as a result of the source-drain thermal coupling.

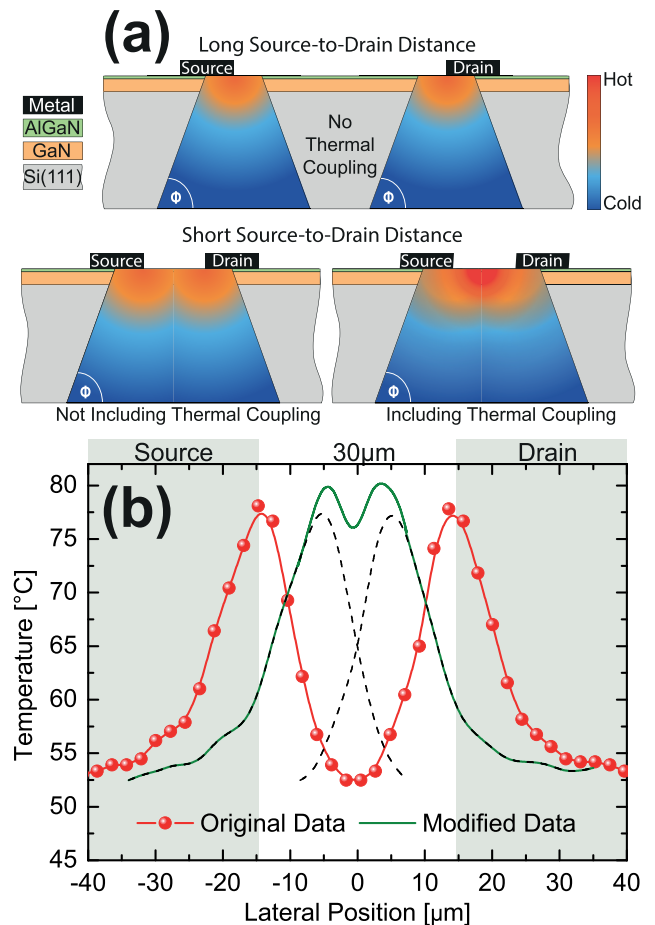


**FIGURE 4.** (a) Illustration of the heat spreading angle and the source/drain thermal coupling in the short and long TLMs. (b) Measured temperature profile along the top surface of the long AlGaIn/GaN TLM ( $L_{SD} = 30 \mu\text{m}$ ) at  $V_{DS} = 12 \text{ V}$ . The original measured data are compared to the modified data to show a very negligible thermal coupling between the inner ends of Ohmic contacts in a long  $L_{SD}$  device.

Unlike in the long TLM, the channel temperature is at its maximum in the center of the short TLM ( $L_{SD} = 10 \mu\text{m}$ ). This can be explained by a heat spread angle and a strong thermal coupling between source and drain, as illustrated in Fig. 4a. The temperature in the middle of the short TLM is much higher than at the inner ends of Ohmic contacts. To demonstrate the low thermal coupling in the long TLM ( $L_{SD} = 30 \mu\text{m}$ ), we have artificially modified the measured temperature profile by reducing the source-to-drain distance from  $30 \mu\text{m}$  to  $10 \mu\text{m}$  (Fig. 4b). It can be seen that the resultant temperature profile (modified data) is slightly larger than the original data but still present two peaks, in contrary to the measured temperature of the short TLM ( $L_{SD} = 10 \mu\text{m}$ ).

The channel temperatures of the AlGaIn/GaN TLMs are plotted against the dissipated power density in Fig. 5. The dissipated power density is controlled via  $V_{DS}$ . For a given dissipated power density, the temperature is higher in the

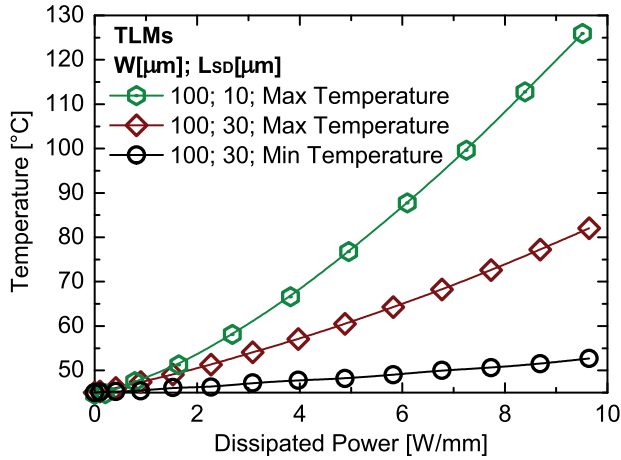


**FIGURE 5.** Evolution of the channel temperature versus the dissipated power density of the AlGaIn/GaN TLMs ( $L_{SD} = 10 \mu\text{m}$  and  $L_{SD} = 30 \mu\text{m}$ ). The Max Temperatures are extracted at the vicinity of S/D contacts for the long TLM and in the center of the device for the short TLM. The Min Temperature corresponds to the value of temperature at center of the long TLM ( $L_{SD} = 30 \mu\text{m}$ ).

short TLM ( $L_{SD} = 10 \mu\text{m}$ ) due to (i) a higher electric field [10] and (ii) a stronger thermal coupling between source and drain sides (Fig. 4a).

To get a rough estimate of the thermal resistance of each TLM, we have employed an analytical thermal model described by the following equation [11], [12]:  $T = T_{SUB} + R_{TH} \times P_{DISS}$ ; where  $T$  is the channel temperature,  $T_{SUB}$  is the substrate temperature ( $45^\circ\text{C}$ ),  $R_{TH}$  is the thermal resistance, and  $P_{DISS}$  is the dissipated power, which is proportional to electric field ( $E$ ), current ( $I_{DS}$ ) and source-to-drain distance ( $L_{SD}$ ):  $P_{DISS} \approx E \times I_{DS} \times L_{SD}$ . According to this model, the increase of  $L_{SD}$  should lead to an increase in channel temperature, due to a larger amount of material for heat to dissipate through. This is in disagreement with experimental observations. Therefore, the temperature increase with the reduction of  $L_{SD}$  is mainly caused by the thermal resistance. With respect to the heat spreading angle model [13]–[15], as illustrated in Fig. 4a, the thermal resistance increases with decreased  $L_{SD}$  due to the less substrate volume for heat to dissipate. The extracted thermal resistance are  $68^\circ\text{C W}^{-1}$  and  $38^\circ\text{C W}^{-1}$  for short ( $L_{SD} = 10 \mu\text{m}$ ) and long ( $L_{SD} = 30 \mu\text{m}$ ) TLMs, respectively. These values of  $R_{TH}$  are within the typical range of values [16], [17]. Here, we have used the maximum temperatures that occur (i) at the inner-ends of the source and drain terminals for the long TLM ( $L_{SD} = 30 \mu\text{m}$ ) and (ii) in the center of the device for the short TLM ( $L_{SD} = 10 \mu\text{m}$ ), due to thermal coupling. When using temperature values in the middle of the TLM with  $L_{SD} = 30 \mu\text{m}$  (Min Temperature), the extracted  $R_{TH}$  is equal to  $9.0^\circ\text{C W}^{-1}$ , over three times smaller than at the inner-ends of the source and drain terminals. This is an indication of a non-uniform distribution of the electric field between source and drain contacts.

It has been reported that the S/D Ohmic contacts process annealing and device operation induce mechanical stress

due to (i) a mismatch in thermal expansion coefficients of III-N and Ti/Al/Ni/Au metallization scheme, and (ii) an exacerbation of inverse piezoelectric effect at high temperatures [18]–[20]. These effects result in a change of strain at the vicinity of metal contacts. The deformation of  $c$ -plane nitride crystal under compressive and tensile strains [22] around the contacts is illustrated in Fig. 6b.

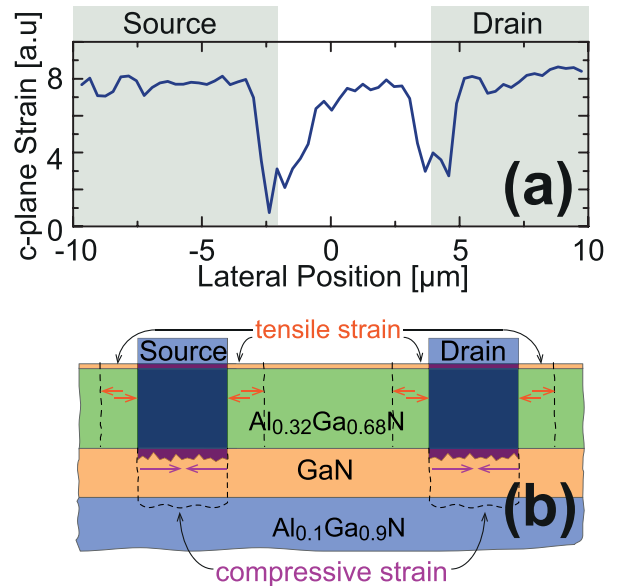


**FIGURE 6.** (a) Measured strain in the channel along the lateral direction of an AlGaIn/GaN TLM using synchrotron radiation-based High-Resolution X-RAY Diffraction (HRXRD), showing a reduction of strain at the inner ends of S/D contacts. (b) The schematic of strain distribution at the vicinity of S/D Ohmic contacts.

The above theory is supported by the strain profile, measured by HRXRD and given in Fig. 6a, that reveals a reduction of strain at the inner ends of S/D contacts. The strain reduction at the inner ends of the contacts diminishes the electron density at these locations which, in turn, increases the electric field locally [23], hence an increase in channel temperature.

The impact of the strain reduction, at the inner ends of S/D Ohmic contacts, on the device electrostatic has been investigated by DD simulations and HRXRD measured data. The lateral 2DEG profile overlapped with corresponding potential distribution at  $V_{DS} = 0 \text{ V}$ , when taking into account the measured strain, are shown in Fig. 7a. At least 25 % reduction in 2DEG density is observed at the inner ends of S/D contacts, as result of strain degradation. Figs. 8a and 8b compare the simulated electric field distributions with measured temperature profiles under  $V_{DS} = 12 \text{ V}$  for both short ( $L_{SD} = 10 \mu\text{m}$ ) and long ( $L_{SD} = 30 \mu\text{m}$ ) TLMs, respectively. Electric field peaks, that occur at the inner ends of the S/D contacts, are nearly three times larger than that at the middle of the device and directly correlate with the measured temperature profiles. As the electric field and the drain current increase proportionally with  $V_{DS}$ , the channel temperature increases near the Ohmic contacts. With the proportional relationship between electric field and temperature,

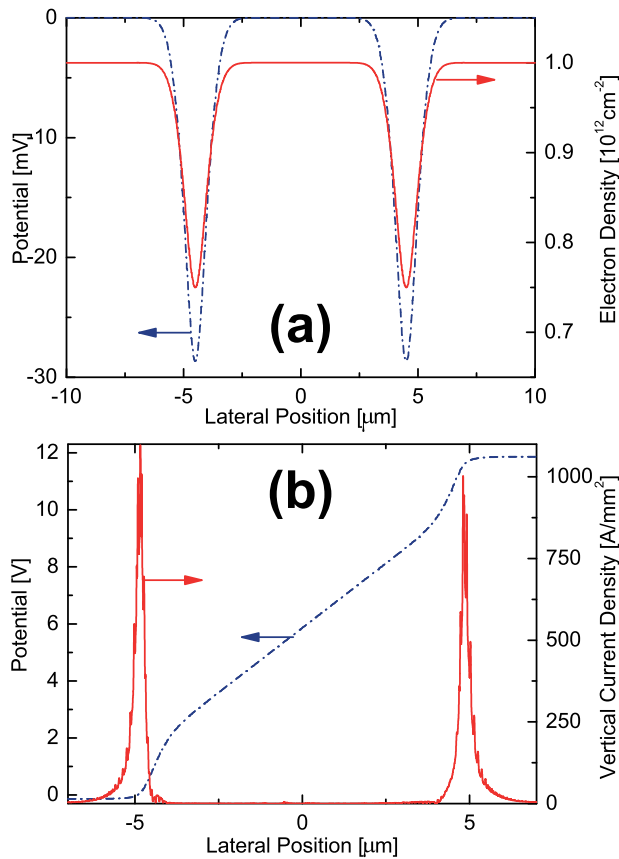


**FIGURE 7.** Drift-Diffusion (DD) simulation results of the short TLM ( $L_{SD} = 10 \mu\text{m}$ ), when taking into account the HRXRD measured strain. (a) Lateral 2DEG profile overlapped with potential distribution at  $V_{DS} = 0 \text{ V}$  in the channel of the TLM. (b) Vertical current density overlapped with potential distribution at  $V_{DS} = 12 \text{ V}$  in the channel of the TLM.

the degradation of strain significantly impacts temperature peaks within the device. Furthermore, the simulated vertical current density, given in Fig. 7b, shows that the majority of current flows in/out of the 2DEG through a small portion of the S/D contacts as suggested by Trilayer-TLM model Ohmic contacts [29]. This attribute could be a cause of a further strain degradation and channel temperature increase.

### B. AlGaIn/GaN GATED DEVICES

It was not possible to observe the temperature peaks at the vicinity of the Ohmic contacts in AlGaIn/GaN HEMTs due (i) to the strong thermal coupling between contacts when  $L_{SD} \leq 10 \mu\text{m}$ , as demonstrated in the previous section; and (ii) to the hot-spot at the end of the gate, as described in this section. However, a temperature rise near source and drain contacts still take place in HEMTs, since the fabrication process of Ohmic contacts in gated and gateless devices are exactly the same. We shall therefore expect to observe temperature rise near the source/drain contacts in HEMTs as in TLMs.

The  $I_D$ - $V_G$  characteristics of two AlGaIn/GaN HEMTs with different configurations (single or two-finger gate) are

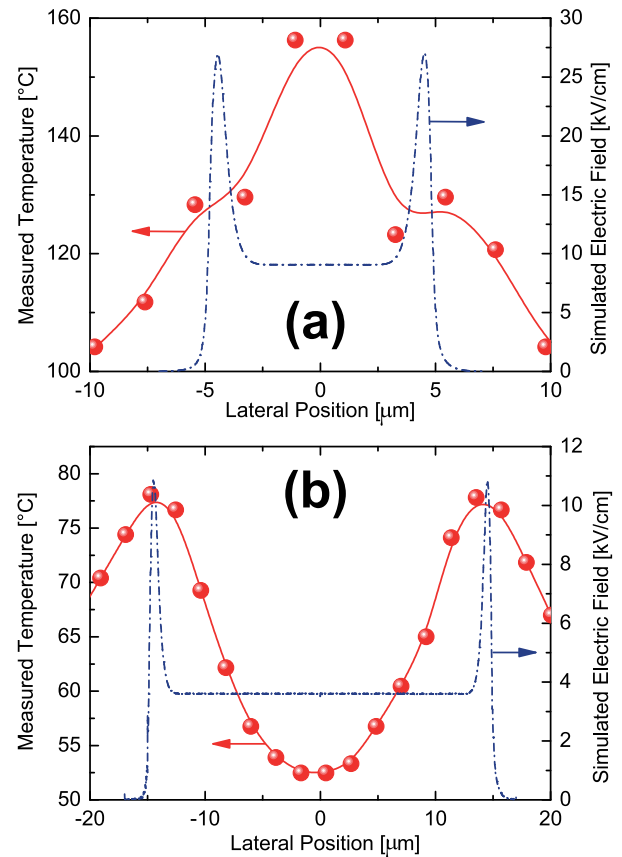


**FIGURE 8.** Simulated electric field distributions and measured temperature profiles at  $V_{DS} = 12 \text{ V}$  of (a) short TLM ( $L_{SD} = 10 \mu\text{m}$ ) and (b) long TLM ( $L_{SD} = 30 \mu\text{m}$ ).

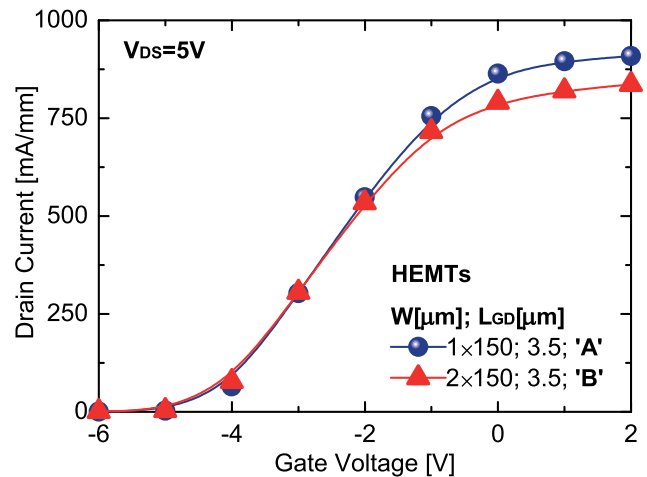


**FIGURE 9.** Measured  $I_D$ - $V_G$  characteristics of single and two-finger gate AlGaIn/GaN HEMTs at  $V_{DS} = 5 \text{ V}$ . The device dimensions are:  $L_{SG} = 1.0 \mu\text{m}$ ,  $L_G = 0.5 \mu\text{m}$ ,  $L_{GD} = 3.5 \mu\text{m}$ .

presented in Fig. 9. The two-finger gate device 'B' outputs less current than single-finger gate HEMT 'A', a point to be noted in discussion. The same temperature measurement technique is applied to a two-finger gate HEMT with  $L_{GD} = 2.5 \mu\text{m}$  and  $W = 2 \times 150 \mu\text{m}$  (Fig. 10a). Since  $L_{SD}$  of

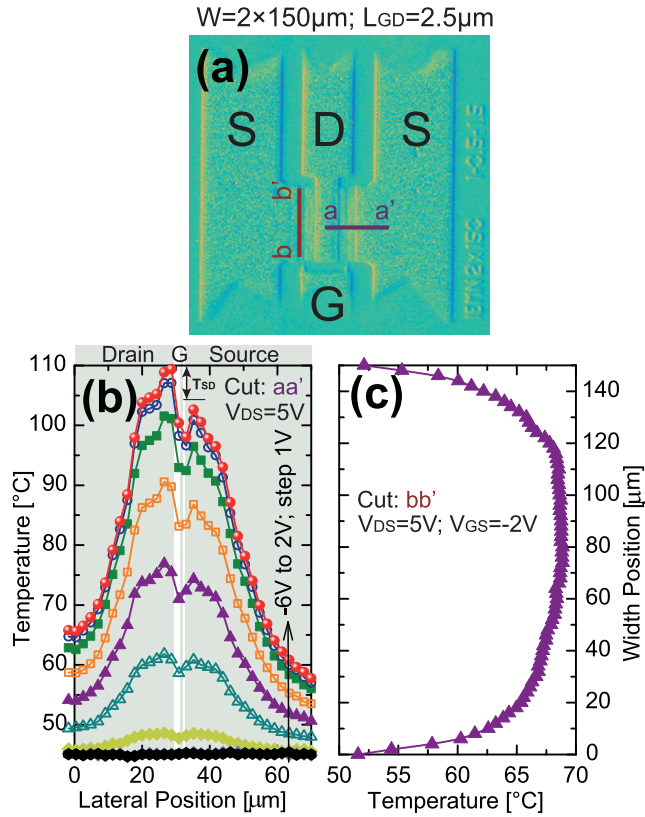


**FIGURE 10.** (a) Layout of two-finger gate AlGaIn/GaN HEMTs. (b) Measured temperature profiles at  $V_{DS} = 5\text{ V}$  and at different gate voltages ( $-6\text{ V}$  to  $2\text{ V}$ ; step  $1\text{ V}$ ) along the lateral position (Cut:  $aa'$ ). (c) Temperature distribution at  $V_{DS} = 5\text{ V}$  and  $V_{GS} = -2\text{ V}$  along the width position (Cut:  $bb'$ ). The device dimensions are:  $L_{SG} = 1.0\ \mu\text{m}$ ,  $L_G = 0.5\ \mu\text{m}$ ,  $L_{GD} = 2.5\ \mu\text{m}$ . Same phenomena have been observed for HEMT with  $L_{GD} = 3.5\ \mu\text{m}$ .

this device is less than  $10\ \mu\text{m}$ , the peaks of temperature at the inner ends of S/D contacts are merged together. This profile is similar to what has already been reported in literature using techniques such as  $\mu\text{Raman}$  [30]. The notch between the source and drain sides is caused by the metal gate. In addition, a higher temperature peak can also be seen at the end of the gate (toward the drain side, as marked by  $T_{SD}$  in Fig. 10b). This peak may be slightly undervalued, due to the limited resolution of the IR System. The drain-side temperature increase as  $V_{GS}$  increases can be explained by the temperature coupling with that of the neighboring HEMT and by the high electron kinetic energy at the end of the gate [31].

The maximum device temperatures of the AlGaIn/GaN HEMTs are plotted against dissipated power density in Fig. 11a. The dissipated power density is controlled via  $V_{GS}$  and  $V_{DS}$ . The presence of temperature coupling between two neighboring HEMTs (two-finger gate HEMT 'B':  $W = 2 \times 150\ \mu\text{m}$ ), due to heat spreading angle as illustrated in Fig. 11b, leads to channel temperature increase, when compared with a single-gate HEMT ('A':  $W = 1 \times 150\ \mu\text{m}$ ) [32]. As results, the two-finger gate exhibits lower drain current as shown in Fig. 9 [24],

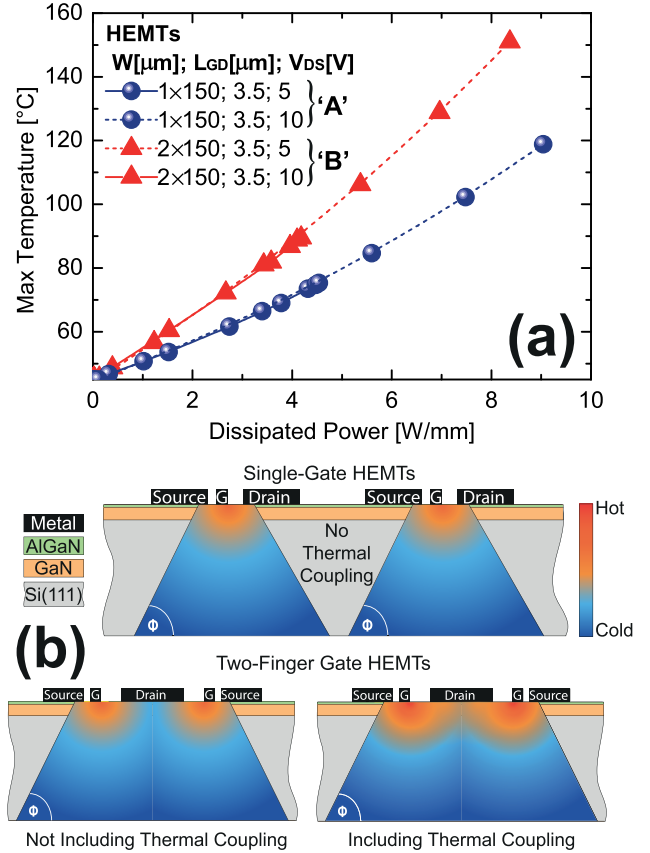


**FIGURE 11.** (a) Evolution of the maximum channel temperature versus the dissipated power density of single and two-finger gate AlGaIn/GaN HEMTs ('A':  $W = 1 \times 150\ \mu\text{m}$ ; and 'B':  $W = 2 \times 150\ \mu\text{m}$ ). The device dimensions are:  $L_{SG} = 1.0\ \mu\text{m}$ ,  $L_G = 0.5\ \mu\text{m}$ ,  $L_{GD} = 3.5\ \mu\text{m}$ . (b) Illustration of the heat spreading angle in single and two-finger gate AlGaIn/GaN HEMTs.

opposite to the expected higher current without considering thermal coupling. This experimental observation is in good agreement with heat spreading angle models [13]–[15]. The main cause of temperature rise in AlGaIn/GaN HEMT is, therefore, the high value of the electric field at the end of the gate toward the drain side. The electrons that enter the device via the source terminal and crystal lattice of AlGaIn and GaN gain significant energy at the drain-side gate edge, due to the large electric field peak in the local area. Consequently, a non-uniform distribution of dissipated power produces a hot spot of temperature to be formed at this location [33]–[35]. This phenomenon happens regardless of the strain reduction near the contact [36], [37]. Therefore, the physics behind temperature rise near the gate and near source/drain contacts are very different. Both mechanisms contribute to the higher temperature at the drain side in AlGaIn/GaN HEMTs. Further investigation will be needed to separate the thermal effects of the two mechanisms in this device.

#### IV. CONCLUSION

Infrascopy temperature mapping system measurements have shown a large increase in temperature at the S/D contacts

of AlGaIn/GaN-based devices at operating conditions. Temperature coupling of a high conductivity tensile region to the lower conductivity regions is responsible for the temperature rise observed in both short and long gateless devices. The thermal coupling also enhances the peak of temperature at the end of the gate in the AlGaIn/GaN HEMTs. In addition, the HRXRD measurement supported by DD simulations have revealed that the change of the strain at the vicinity of S/D Ohmic contacts, due to a difference in expansion coefficients of III-N and S/D metallization, is the reason behind this temperature rise.

## REFERENCES

- [1] D. W. Runtton, B. Trabert, J. B. Shealy, and R. Vetry, "History of GaN: High-power RF gallium nitride (GaN) from infancy to manufacturable process and beyond," *IEEE Microw. Mag.*, vol. 14, no. 3, pp. 82–93, Apr. 2013, doi: [10.1109/MMM.2013.2240853](https://doi.org/10.1109/MMM.2013.2240853).
- [2] J. J. Komiak, "GaN HEMT: Dominant force in high-frequency solid-state power amplifiers," *IEEE Microw. Mag.*, vol. 16, no. 3, pp. 97–105, Apr. 2015, doi: [10.1109/MMM.2014.2385303](https://doi.org/10.1109/MMM.2014.2385303).
- [3] M. A. Khan, A. Bhattarai, J. N. Kuznia, and D. T. Olson, "High electron mobility transistor based on a GaN  $\text{Al}_x\text{Ga}_{1-x}\text{N}$  heterojunction," *Appl. Phys. Lett.*, vol. 63, pp. 1214–1215, Mar. 1993, doi: [10.1063/1.109775](https://doi.org/10.1063/1.109775).
- [4] J. Wuerfl *et al.*, "Reliability issues of GaN based high voltage power devices," *Microelectron. Reliab.*, vol. 51, pp. 1710–1716, Sep. 2011, doi: [10.1016/j.microrel.2011.07.017](https://doi.org/10.1016/j.microrel.2011.07.017).
- [5] G. Meneghesso *et al.*, "Reliability and parasitic issues in GaN-based power HEMTs: A review," *Semicond. Sci. Technol.*, vol. 31, no. 9, p. 093004, Aug. 2016, doi: [10.1088/0268-1242/31/9/093004](https://doi.org/10.1088/0268-1242/31/9/093004).
- [6] G. Meneghesso *et al.*, "Reliability issues of gallium nitride high electron mobility transistors," *Int. J. Microw. Wireless Technol.*, vol. 2, no. 1, pp. 39–50, Feb. 2010, doi: [10.1017/S1759078710000097](https://doi.org/10.1017/S1759078710000097).
- [7] A. Soltani *et al.*, "Power performance of AlGaIn/GaN high-electron-mobility transistors on (110) silicon substrate at 40 GHz," *IEEE Electron Device Lett.*, vol. 34, no. 4, pp. 490–492, Apr. 2013, doi: [10.1109/LED.2013.2244841](https://doi.org/10.1109/LED.2013.2244841).
- [8] R. A. Hopper and C. H. Oxley, "Improved infrared imaging of semiconductor devices," in *Advances in Scientific Research and Education*. Badajoz, Spain: Formatex Research Center, 2014, pp. 697–702.
- [9] P. W. Webb and I. A. D. Russell, "Thermal simulation of transients in microwave devices," *IEE Proc. G Circuits, Devices Syst.*, vol. 138, no. 3, pp. 329–334, Jun. 1991, doi: [10.1049/ip-g-2.1991.0056](https://doi.org/10.1049/ip-g-2.1991.0056).
- [10] B. Benbakhti, M. Rousseau, A. Soltani, and J. C. De Jaeger, "Analysis of thermal effect influence in gallium-nitride-based TLM structures by means of a transport-thermal modeling," *IEEE Trans. Electron Devices*, vol. 53, no. 9, pp. 2237–2242, Aug. 2006, doi: [10.1109/TED.2005.881014](https://doi.org/10.1109/TED.2005.881014).
- [11] B. K. Schwitter, A. E. Parker, S. J. Mahon, A. P. Fattorini, and M. C. Heimlich, "Impact of bias and device structure on gate junction temperature in AlGaIn/GaN-on-Si HEMTs," *IEEE Trans. Electron Devices*, vol. 61, no. 5, pp. 1327–1334, May 2014, doi: [10.1109/TED.2014.2311660](https://doi.org/10.1109/TED.2014.2311660).
- [12] D. Altman *et al.*, "Analysis and characterization of thermal transport in GaN HEMTs on diamond substrates," in *Proc. 14th Intersoc. Conf. Therm. Thermomech. Phenom. Electron. Syst.*, 2014, pp. 1199–1205, doi: [10.1109/ITHERM.2014.6892416](https://doi.org/10.1109/ITHERM.2014.6892416).
- [13] D. Schweitzer and L. Chen, "Heat spreading revisited—Effective heat spreading angle," in *Proc. Therm. Meas. Modeling Manage. Symp.*, 2015, pp. 88–94, doi: [10.1109/SEMI-THERM.2015.7100145](https://doi.org/10.1109/SEMI-THERM.2015.7100145).
- [14] C. J. M. Lasance, "Heat spreading: Not a trivial problem," *Electron. Cooling*, vol. 14, no. 2, p. 24, 2008.
- [15] D. Schweitzer and L. Chen, "Heat spreading revisited—Effective heat spreading angle," in *Proc. 31th SEMITHERM*, San Jose, CA, USA, 2015, pp. 88–94.
- [16] R. Sommet, G. Mouginot, R. Quere, Z. Ouarch, and M. Camiade, "Thermal modeling and measurements of AlGaIn/GaN HEMTs including thermal boundary resistance," *Microelectron. J.*, vol. 43, no. 9, pp. 611–617, Sep. 2012, doi: [10.1016/j.mejo.2011.07.009](https://doi.org/10.1016/j.mejo.2011.07.009).
- [17] C. K. Yang *et al.*, "Pulsed-IV pulsed-RF cold-FET parasitic extraction of biased AlGaIn/GaN HEMTs using large signal network analyzer," *IEEE Trans. Microw. Theory Techn.*, vol. 58, no. 5, pp. 1077–1088, May 2010, doi: [10.1109/TMTT.2010.2045452](https://doi.org/10.1109/TMTT.2010.2045452).
- [18] C.-H. Lin *et al.*, "Strain and temperature dependence of defect formation at AlGaIn/GaN high-electron-mobility transistors on a nanometer scale," *IEEE Trans. Electron Devices*, vol. 59, no. 10, pp. 2667–2674, Oct. 2012, doi: [10.1109/TED.2012.2206595](https://doi.org/10.1109/TED.2012.2206595).
- [19] J. Joh and J. A. del Alamo, "Critical voltage for electrical degradation of GaN high-electron mobility transistors," *IEEE Electron Device Lett.*, vol. 29, no. 4, pp. 287–289, Apr. 2008, doi: [10.1109/LED.2008.917815](https://doi.org/10.1109/LED.2008.917815).
- [20] K. R. Bagnall, E. A. Moore, S. C. Badescu, L. Zhang, and E. N. Wang, "Simultaneous measurement of temperature, stress, and electric field in GaN HEMTs with micro-Raman spectroscopy," *Rev. Sci. Instrum.*, vol. 88, no. 11, pp. 113111-1–113111-16, 2017, doi: [10.1063/1.5010225](https://doi.org/10.1063/1.5010225).
- [21] P. L. Bonanno *et al.*, "Submicron beam X-ray diffraction of nanoheteroepitaxially grown GaN: Experimental challenges and calibration procedures," *Nucl. Instrum. Methods Phys. Res. B, Beam Interact. Mater. At.*, vol. 268, no. 3–4, pp. 320–324, Feb. 2010.
- [22] D. Zhu, D. J. Wallis, and C. J. Humphreys, "Prospects of III-nitride Optoelectronics grown on Si," *Rep. Prog. Phys.*, vol. 76, no. 10, p. 106501, Oct. 2013, doi: [10.1088/0034-4885/76/10/106501](https://doi.org/10.1088/0034-4885/76/10/106501).
- [23] A. Wang *et al.*, "Impact of intrinsic stress in diamond capping layers on the electrical behavior of AlGaIn/GaN HEMTs," *IEEE Trans. Electron Devices*, vol. 60, no. 10, pp. 3149–3156, Oct. 2013, doi: [10.1109/TED.2013.2275031](https://doi.org/10.1109/TED.2013.2275031).
- [24] B. Benbakhti, A. Soltani, K. Kalna, M. Rousseau, and J.-C. De Jaeger, "Effects of self-heating on performance degradation in AlGaIn/GaN-based devices," *IEEE Trans. Electron Devices*, vol. 56, no. 10, pp. 2178–2185, Oct. 2009, doi: [10.1109/TED.2009.2028400](https://doi.org/10.1109/TED.2009.2028400).
- [25] M. Rousseau, A. Soltani, and J. C. De Jaeger, "Efficient physical-thermal model for thermal effects in AlGaIn/GaN high electron mobility transistors," *Appl. Phys. Lett.*, vol. 101, no. 12, p. 122101, 2012, doi: [10.1063/1.4753815](https://doi.org/10.1063/1.4753815).
- [26] K. Ahmeda *et al.*, "Role of self-heating and polarization in AlGaIn/GaN-based heterostructures," *IEEE Access*, vol. 5, pp. 20946–20952, Oct. 2017, doi: [10.1109/ACCESS.2017.2755984](https://doi.org/10.1109/ACCESS.2017.2755984).
- [27] B. Benbakhti, M. Rousseau, and J. C. De Jaeger, "Study of field plate AlGaIn/GaN HEMTs by means of a 2D-hydrdynamic model for power applications," in *Proc. Eur. Microw. Integr. Circuits Conf.*, 2006, pp. 363–366, doi: [10.1109/EMICC.2006.282657](https://doi.org/10.1109/EMICC.2006.282657).
- [28] F. Dessenne, D. Cichocka, P. Desplanques, and R. Fauquembergue, "Comparison of wurtzite and zinc blende III-V nitrides field effect transistors: A 2D Monte Carlo device simulation," *Mater. Sci. Eng., B*, vol. 50, nos. 1–3, pp. 315–318, Dec. 1997, doi: [10.1016/S0921-5107\(97\)00197-9](https://doi.org/10.1016/S0921-5107(97)00197-9).
- [29] J. C. Gerbedoen, "Conception et réalisation technologique de transistors de la filière HEMTs AlGaIn/GaN sur substrat silicium pour l'amplification de puissance hyperfréquence," Ph.D. dissertation, Dept. Inst. Electron., Microelectron. Nanotechnol., Lille Univ. Sci. Technol., Villeneuve-d'Ascq, France, 2009.
- [30] N. Killat *et al.*, "Thermal properties of AlGaIn/GaN HFETs on bulk GaN substrates," *IEEE Electron Device Lett.*, vol. 33, no. 3, pp. 366–368, Mar. 2012, doi: [10.1109/LED.2011.2179972](https://doi.org/10.1109/LED.2011.2179972).
- [31] K. Maize *et al.*, "High resolution thermal characterization and simulation of power AlGaIn/GaN HEMTs using micro-Raman thermography and 800 picosecond transient thermoreflectance imaging," in *Proc. IEEE Compound Semicond. Integr. Circuit Symp.*, Oct. 2014, pp. 1–8, doi: [10.1109/CSICS.2014.6978561](https://doi.org/10.1109/CSICS.2014.6978561).
- [32] A. Darwish, A. J. Bayba, and H. A. Hung, "Channel temperature analysis of GaN HEMTs with nonlinear thermal conductivity," *IEEE Trans. Electron Devices*, vol. 62, no. 3, pp. 840–846, Mar. 2015, doi: [10.1109/TED.2015.2396035](https://doi.org/10.1109/TED.2015.2396035).
- [33] J. Si, J. Wei, W. Chen, and B. Zhang, "Electric field distribution around drain-side gate edge in AlGaIn/GaN HEMTs: Analytical approach," *IEEE Trans. Electron Devices*, vol. 60, no. 10, pp. 3223–3229, Oct. 2013, doi: [10.1109/TED.2013.2272055](https://doi.org/10.1109/TED.2013.2272055).
- [34] V. G. Tikhomirov *et al.*, "Simulation of electric field distribution in GaN HEMTs for the onset of structure degradation," in *Proc. Int. Workshop Electromagn. Compat. Integr. Circuits*, 2017, pp. 115–118, doi: [10.1109/EMCCo.2017.7998094](https://doi.org/10.1109/EMCCo.2017.7998094).
- [35] M. Tapajna *et al.*, "Hot-electron-related degradation in InAlN/GaN high-electron-mobility transistors," *IEEE Trans. Electron Devices*, vol. 61,

no. 84, pp. 2793–2800, Aug. 2014, doi: [10.1109/TED.2014.2332235](https://doi.org/10.1109/TED.2014.2332235).

- [36] R. J. T. Simms, J. W. Pomeroy, M. J. Uren, T. Martin, and M. Kuball, “Channel temperature determination in high-power AlGaIn/GaN HFETs using electrical methods and Raman spectroscopy,” *IEEE Trans. Electron Devices*, vol. 55, no. 2, pp. 478–482, Feb. 2008, doi: [10.1109/TED.2007.913005](https://doi.org/10.1109/TED.2007.913005).
- [37] Z. Yan, G. Liu, J. M. Khan, and A. A. Balandin, “Graphene quilts for thermal management of high-power GaN transistors,” *Nature Commun.*, vol. 3, pp. 827–828, May 2012, doi: [10.1038/ncomms1828](https://doi.org/10.1038/ncomms1828).



**STEVEN J. DUFFY** received the B.Eng. degree in electrical and electronics engineering and the M.Sc. degree in microelectronic systems design from Liverpool John Moores University, in 2014 and 2015, respectively, where he is currently pursuing the Ph.D. degree in reliability characterization of III-nitrides-based devices for technology development. During his M.Sc. project which was supervised by Dr. B. Benbakhti, he developed his interest in the reliability and thermal analysis of GaN-based devices.



**BRAHIM BENBAKHTI** received the M.Sc. and Ph.D. degrees in microwave and microtechnology from Lille University, Lille, France, in 2003 and 2007, respectively. He is currently with the Electronics and Electrical Engineering Department, Liverpool JMU, Liverpool, U.K. His current research interests include reliability characterization and simulation of III-nitrides-based devices and sensors, transistor structure engineering, and nanoscale III-V/Ge CMOS.



co-authored 91 peer-reviewed papers and gave over 20 invited talks.

**KAROL KALNA** received the M.Sc. degree (Hons.) and the Ph.D. degree from Comenius University, Bratislava, in 1990 and 1998, respectively. In 2002, he received the EPSRC Advanced Research Fellowship and pioneered III-V MOSFETs. In 2010, he became a Senior Lecturer with Swansea University, U.K., establishing the Nanoelectronic Devices Computational Group. He is currently an Associate Professor with Swansea University. He has authored or



**MOHAMMED BOUCHERTA** received the master's degree in micro- and nanotechnologies from the Ecole Centrale, Lille, France, in 2015. He is currently pursuing the Ph.D. degree with the Georgia Tech-CNRS, Metz, France, and the Institute of Electronics Microelectronics and Nanotechnology, Villeneuve-d'Ascq, France.



**WEI D. ZHANG** received the Ph.D. degree from Liverpool John Moores University (LJMU), Liverpool, U.K., in 2003. He is currently a Professor of nanoelectronics with LJMU. His current research interests include characterization and quality assessment of resistive switching and flash memory devices, CMOS devices based on Si, Ge, and III-V materials, and GaN high-electron-mobility transistor devices.



microwave circuit. His telecommunications.

**NOUR E. BOURZGUI** is currently an Associate Professor with Lille 1 University. He is a specialist in electrical characterization in the microwave and instrumentation. He is also a specialist in the design and development of biological micro-sensor for the biomolecular analysis in solution by means of microfluidic channels by dielectric spectroscopy in the millimeter and sub-millimeter waves' range. He rejoined the Microwave Power Devices Team in 2015, with expertise on the



**ALI SOLTANI** received the B.Sc. degree in theoretical physics and the M.Sc. degree in optoelectronic from Lorraine University, Nancy, France, in 1994 and 1996, respectively, and the Ph.D. degree in electrical engineering from Metz University and Supélec, Gif-sur-Yvette, France, in 2001. His current research interests include the Al(Ga)N/GaN resonant tunneling diodes, X-UV photodetectors, elastic wave sensors, the design and fabrication of wide bandgap, high-power, and high-frequency devices.

...